Δελτίο της Ελληνικής Γεωλογικής Εταιρίας τομ. XXXVII, 218 -231, 2005
Bulletin of the Geological Society of Greece vol. XXXVII, 218 - 231, 2005

3-D NUMERICAL MODELING ON OVERLAPPING NORMAL FAULT SEGMENTS: A CASE STUDY FROM MEGALOPOLIS BASIN, PELOPONNESE, GREECE

Sourlas G., Kokkalas S. and Koukouvelas I.
Department of Geology, University of Patras, 26500, Patras, Greece.

ABSTRACT

Many normal faults consist of closely spaced overlapping segments. Field data on pre-existing and active faults indicate that such geometries have a pronounced effect on the distribution of the fault slip. The slip distribution on the segments is complex and asymmetric while the area of maximum slip generally is not located at the center of the segment. In relay zones between segments, slip gradients are steeper. Numerical analysis using a 3-D boundary element method was applied in two overlapping normal fault segments observed in the Megalopolis lignite mine. Our analysis suggests that mechanical interaction between neighboring segments may cause such asymmetrical slip distributions. This interaction occurs through local perturbation of the stress field and does not require the segments to be connected. Additionally, 3-D numerical modeling enable us to reproduce the principal characteristics of the observed fault scarps, and to illustrate the variation of the maximum Coulomb shear stress in the surrounding rock volume. In the relay zone a region of high Coulomb stress is observed. In this region, relay breaching deformation is possible to initiate, leading to segment hard linkage. In this way, this kind of modeling provides a mechanical rationale for fault evolution.

1. INTRODUCTION

It has been recognized for many years that major faults consist of arrays of distinct segments rather than a single fault slip plane (Tchalenko & Ambraseys 1970, Moore 1979, Segall & Pollard 1980, Peacock 1991, Peacock & Sanderson 1994). Fault segmentation is observable over a wide range of scales (Pollard and Aydin 1984, Nelson et al. 1992). The mechanical interaction between adjacent segments affects the subsequent development of each segment and the evolution of composite faults, which are comprised of linked segments (Willemse et al. 1996). Initially isolated and non coplanar segments propagate towards each other and interact producing a relay ramp. Connecting fractions start to link by breaching the relay ramp and finally the relay ramp is destroyed to produce a single, irregular fault (Peacock 2002).

Segmentation also plays an important role to the slip distribution across the fault surface. Along a single isolated fault, the slip distribution is relatively symmetric (Fig.1a). Slip varies from zero at tip lines to a relative maximum value near the middle of the fault surface (Rippon 1985, Dawers et al. 1993). However, for segmented fault arrays the slip distribution is generally asymmetric and more complex due to the mechanical interaction between the neighboring segments (Fig.1b). Steep displacement gradients occur at oversteps and points of maximum displacement are commonly shifted away from the center of the fault (Willemse et al. 1996, Crider & Pollard 1998).

In this study, we use 3-D numerical modeling to reproduce the mechanical interaction between two segments of a normal fault affecting the Megalopolis basin. We use 3-D modeling because natural faults are not infinite in one dimension and do not have blade-like shape, as postulated in 2-D models. Additionally, the 3-D fault shape strongly influences the magnitude and the spatial distribu-

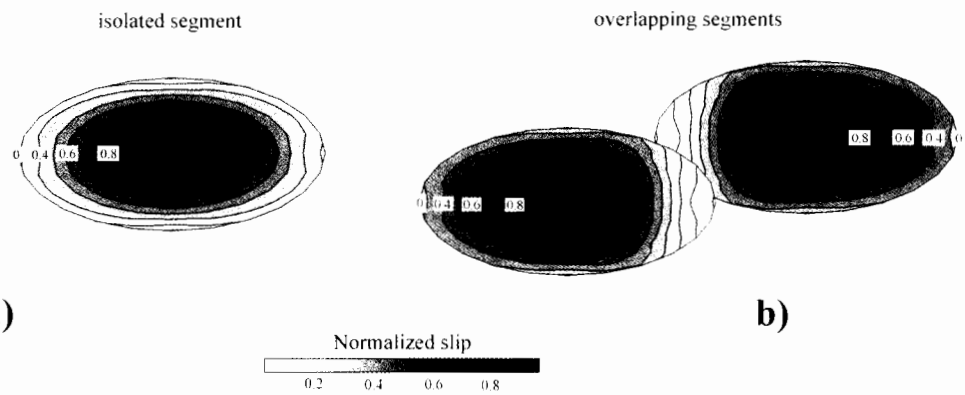

Figure 1. Models for slip distribution on normal faults. a) Slip distribution on a single isolated normal fault. The tip line is elliptical, with contours of equal normalized slip distributed around the displacement maximum in the center of the fault plane. b) Slip distribution on overlapping segments. Slip maximum is located towards the relay zone and the slip gradient is steeper on the relay.

tion of stress enhancement or stress shadowing that cause mechanical interaction (Willemse 1997). Our main purpose is to compare modeling results with observations from a natural segmented normal fault, indicating in this way that field observations can be understood using relatively simple numerical modeling.

2. GEOLOGICAL SETTING

The Megalopolis basin is an intramontane basin located in central Peloponnese and is formed at the boundary between Mesozoic limestones of Pindos unit and Eocene flysch of Tripolitsa unit (Vinken 1965; Fig. 2a). The eastern margin of the basin is marked by a series of NW to NNW trending normal faults, forming a half – graben structure. This fault direction seems to be active since Late Miocene for the area of central and south Peloponnese (Kokkalas et al. 2006, Doutsos and Kokkalas 2001).

Active tectonic subsidence and deposition during the Pliocene and Pleistocene was responsible for the accumulation of a 250 m thick sedimentary sequence. This sequence comprises two large-scale propagation cycles from lacustrine (Makrision and Choremi formations) to fluvial units (Trilofon, Apidhista and Potamia / Thoknia formations; Fig.2a). The lignite deposits in Megalopolis basin have been divided into four major coal seams (Lohnert & Nowak 1965; Fig.2b) intercalated by clay, silt and sand beds. The Choremi formation, which concentrated our main interest (Fig. 2b), consists of lacustrine clays containing freshwater bivalve and ostracod fossils (Hilterman & Luttig 1969), silt and lignite seams ca. 20 m thick (Van Vugt 2000).

The lignite layers exposed in the mines are thickest towards the western part of the basin where subsidence was moderate, enabling swaps to accumulate the organic material for longer periods of time in contrast to the eastern part where tectonic footwall uplift was responsible for the accumulation of the thicker detrital sedimentary units.

3. NUMERICAL MODELING

Our modeling study uses the computer software Poly3d (Thomas 1993), a boundary element method numerical code based on the displacement discontinuity method and the governing equations of linear elasticity theory. Becker (1992) provides a detailed overview of the boundary element technique and Thomas (1993) describes the implementation in Poly3d software. The fundamental solution used by Poly3d is that of an angular dislocation on a homogenous linear elastic half space (Comninou & Dunders 1975, Jeyakumaran et al.

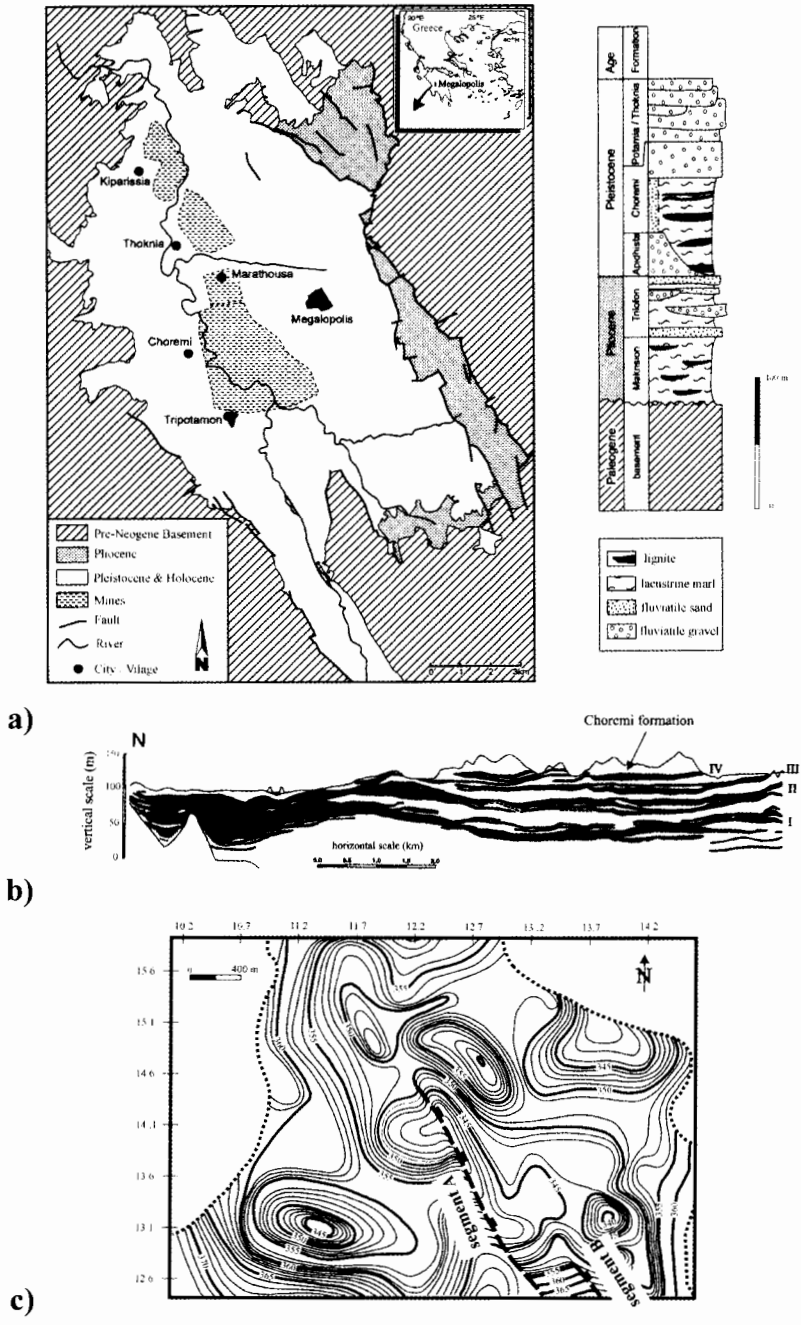

Figure 2. a) Geological map of the Megalopolis basin and stratigraphic column of the basin fill (from Van Vugt 2000). b) Cross section through the Megalopolis basin. Roman numerals indicate the major coal seams (from Van Vugt 2000). c) Topographic map of the study area.

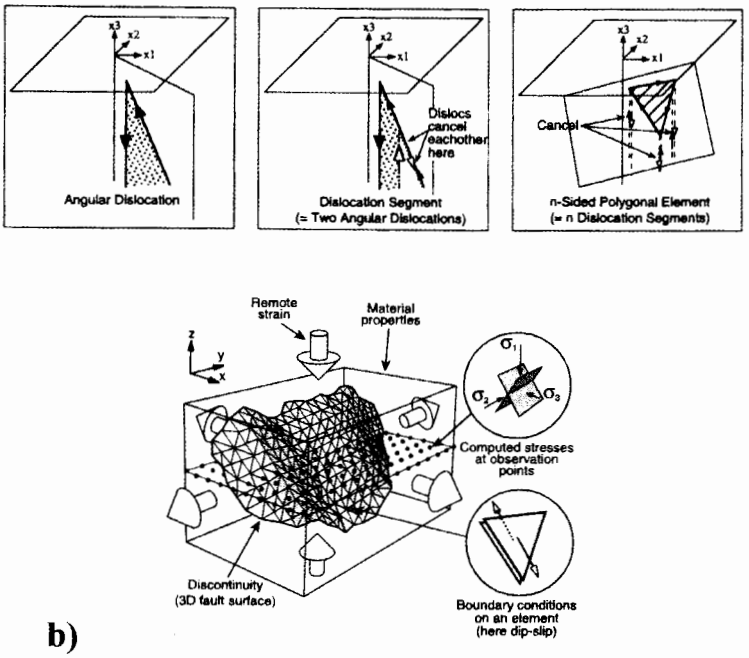

Figure 3. Schematic representation of a Poly3D model configuration. a) Construction of polygonal element is based on the elementary solution of an angular dislocation (left). Two angular dislocations are added to define a dislocation segment (middle). The n dislocation segments are subsequently added to form an n-sided polygonal element (right). b) The discretization of 3D fault surface into triangular boundary elements allows the construction of a surface of any desired tip line shape. Boundary conditions can be applied remotely and locally, at the center of each element. Output at observations points can be displacement, stress and strain (Thomas, 1993).

1992). Two angular dislocations of opposite sign are added to compose a dislocation segment. Several dislocation segments with vertices in a common plane can in turn be superposed to yield a planar polygonal element of constant displacement discontinuity or slip (Fig. 3a). By joining many elements, one or more faults with varying slip can be modeled. Slip varies over the entire fault surface according to a set of step functions. Because the displacement discontinuity is constant across each element, smooth fault slip distributions can be approximated by using many small elements. The faults do not need to be planar and can have irregular tip lines. All modeled faults are imbedded in an infinite homogenous material (Fig. 3b).

The stress, strain tensor and the displacement field at any area of observation points can be calculated in the surrounding material once the slip distribution on the fault surface is known. From the stress tensor and the principal stresses, the maximum Coulomb shear stress or other criteria of failure can be calculated. We used the maximum Coulomb shear stress, ΔS_c, (Jaeger & Cook 1979) as an index for near fault deformation. The value of the maximum Coulomb shear stress is determined by

$$\Delta S_c = \left[\frac{(\sigma_1 - \sigma_3)}{2}\sqrt{1+\mu^2}\right] + \mu\left[\frac{(\sigma_1 + \sigma_3)}{2}\right] \quad (1)$$

where σ_1 and σ_3 are the maximum and minimum principal stresses and μ is the coefficient of internal friction, taken to be 0.6 (after Byerlee 1978). Regions with increased values of ΔS_c rela-

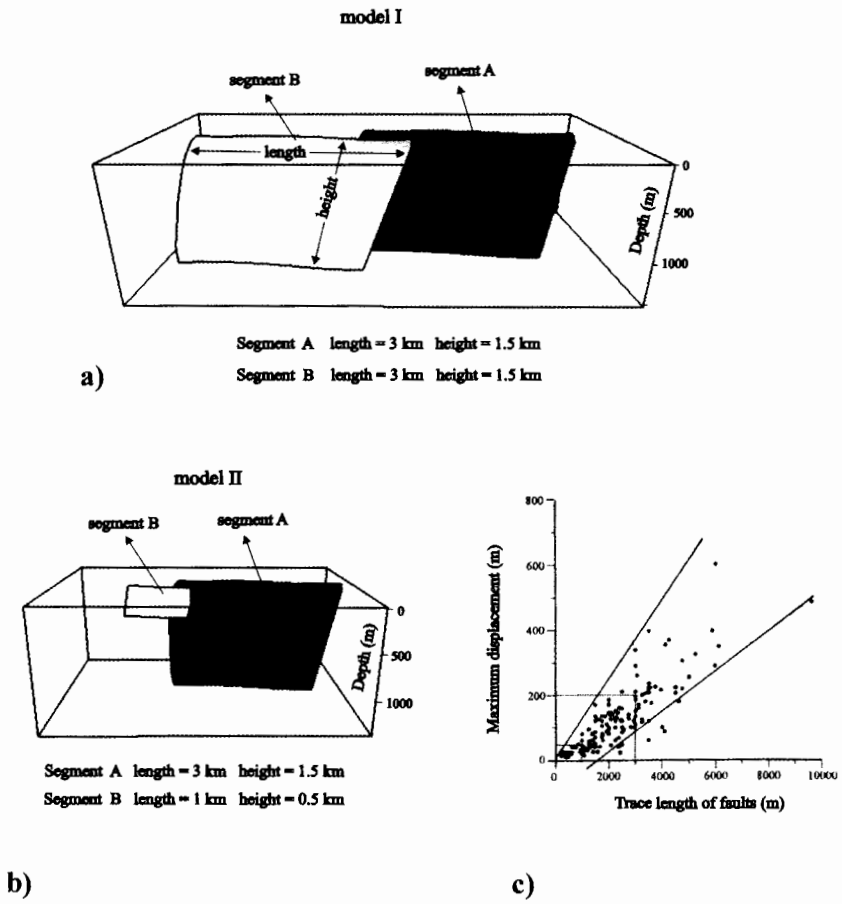

Figure 4. a) First model consisting of two similar sized segments. b) Second model with different sized segments. c) Displacement against length plot (from Koukouvelas et al. 1999). Shaded area indicates the values of interest.

tive to initial conditions are regions where one expects to see future deformation that could contribute to fault propagation and linkage across a ramp (Crider & Pollard 1998).

4. CASE STUDY

In this study, we focused in two overlapping segments of a normal fault affecting the Megalopolis basin (Fig. 2c). Both segments trend parallel, have a NW-SE orientation and have a dip of 55 degrees towards NE. The overlap of the fault segments, defined as the horizontal distance between the two overstepping and proximal segment terminations measured parallel to strike, is 400 m and the spacing, defined as the horizontal distance between the segment surfaces measured perpendicular to their strike, is 350 m. Both segments do not reach the surface. The 3-D geometry of the first segment (segment A) is determined by examining a series of horizontal sections (topographic maps) at different depths derived from the Choremi coal mine. The fault segment has a length of 3 km at the depth of 35 m, its maximum downdip dimension is 1.5 km (aspect ratio=2) and it has a complex 3-D shape. The geometry and the length of the second segment (segment B) could not be fully determined from the field data because excavation and mapping have not reached this mine area. For this reason two

different models were made.

In the first model (model I), the two segments were assumed to have the same dimensions and geometry (Fig. 4a). In the second model (model II), the segment B was assumed to be smaller having a length of 1 km and a maximum downdip dimension of 500 m (aspect ratio=2; Fig. 4b) in order to observe distinct reasonable difference between the two models.

In both models the segments were embedded in a homogenous linear elastic half space. The boundary of the half space represents the traction free surface of the Earth (Fig. 4). Two elastic constants, Poisson's ratio and Young's modulus, were used to characterize the behavior of the surrounding material. For this study, all model calculations use a Poisson ratio of 0.30 and a Young's modulus of 25000 MPa, which are typical values for Neogene deposits (Poulimenos & Doutsos 1997).

Deformation is driven by a uniform, uniaxial tension, of magnitude T, acting perpendicular to the strike of the segments. In this study we chose a value of 10 MPa for the tension magnitude T (after Crider & Pollard 1998). Mechanical interaction between the two segments is modeled by prescribing traction boundary conditions at the center of each element. The displacement discontinuity across each element is found by solving a series of linear algebraic equations that describe the influence of each element on all other elements (Crouch & Starfield 1983). It is important to recognize that normal faults subject to orthogonal extension may experience some strike slip motion due to their 3-D tip lines shapes and mechanical interaction with adjacent segments. But since maximum dip slip motion is about four times greater than maximum strike slip motion, strike slip motion can be ignored (Crider & Pollard 1998). Additionally, the displacement discontinuity perpendicular to the fault was prescribed to be zero, thereby preventing opening and no friction was used on the segment surfaces. Lack of friction is not realistic, but it allows us to observe one end-member of fault behavior: the maximum possible slip and the maximum fault interaction (Crider 2001). These boundary conditions generate a complete downdip displacement discontinuity on both segments surfaces and should be consider a first approximation that will nonetheless capture some of the principal effects of mechanical interaction. For example, Aydin and Schultz (1990) incorporated a Coulomb friction criterion on the fault and showed that the slip distributions for the faults with and without friction are very similar.

The above mentioned conditions reflect the mechanics of an idealized single slip event. A single slip event displaces the surface of the half space, producing fault scarps and variations in the local topography. Comparing the modeled surface displacements with the displacement contours produced from the coal mine data, we can examine which model reproduces the reality with more precision. However, the final topography is not the result of only one slip event. A single slip event can produce an average displacement from few centimeters to meter, for segments of the predefined dimensions, thus many hundreds of events are necessary to reproduce the final topography.

In our case using numerical modeling for a single slip event, the applied orthogonal extension produces maximum displacement of about 0.2 m and 0.035 m for the 3 km and 1 km length segments, respectively. According to Koukouvelas et al. (1999) fault segments with these dimensions have total maximum displacement ca. 200 and 30 m, respectively (Fig. 4c). For this reason we use 1000 events to obtain total maximum displacement values that fit well with the ones obtained from the empirical diagrams of maximum displacement versus length for same dimension fault segments (Koukouvelas et al. 1999).

5. MODEL RESULTS

Once the boundary conditions have been determined, numerical modeling calculates the displacement discontinuity on each element of the segments for a single slip event. Summing the displacement discontinuities of 1000 events, we

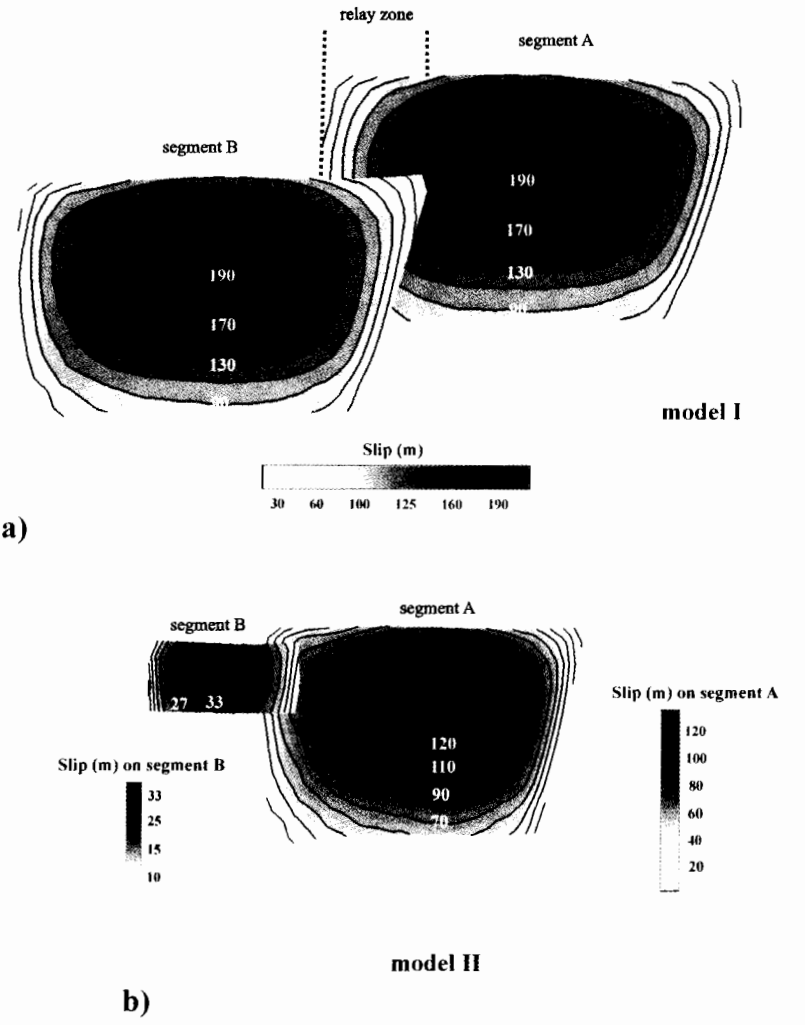

Figure 5. Distribution of dip slip on the modeled fault segments. a) Model I with the similar sized overlapping segments. Contours interval is 20m. Darker areas indicate greater values of slip. b) Model II. Contour interval is 3m and 10m for the segment B and segment A respectively.

determine the slip distribution on the segments. Then, the three components of the displacement field, the stress tensor, the principal stresses and the maximum Coulomb shear stress can be calculated at different observations points in the surrounding rock volume.

5.1 SLIP DISTRIBUTION

In model I on both segments the maximum computed slip is ca. 200 m. The area of maximum slip is shifted from the segment centers towards the area of overlap. The slip gradient is more gentle on the distal parts of the segments and steeper towards the relay zone. The slip is gradually minimized to zero towards the tip lines. In the relay zone the slip gradient decreases rapidly indicating progressive growth impediment with increasing fault overlap. The contours of the computed

slip distribution on the segments are shown in Fig.5a.

Slip distribution on different dimension fault segments is shown in model II (Fig.5b). The main difference between the two models is that since the segment B has smaller dimensions, the mechanical interaction between the two segments is weaker. Thus the maximum slip on the segment A is ca. 130 m, while on the segment B is ca. 35 m. On the segment A the slip gradient is more gentle towards the relay zone and steeper on the distal part while the area of maximum slip is shifted away from the center towards the distal part. This distribution indicates progressive growth of the segments toward the overlap zone which results in stronger mechanical interaction between the segments. Slip distribution on the segment B is approximately symmetrical and the area of the maximum slip is slightly shifted from the center.

5.2 FAULT SCARP SHAPES

In order to investigate which model corresponds better with the field observations, we compared the modeled surface displacements produced by the accumulated slip on the faults over many slip events, with the field data derived from the Choremi coal mine. The field data consist of the upper horizon contour map of the coal seam III (Fig.2b) and were provided by the Puplic Power Corporation. Since the environment of deposition was lacustrine, erosion or scarp degradation have not greatly modified the local topography. For this reason the elevation contours of the upper coal horizon can be used for the comparison with the modeled topography. To facilitate comparisons, the surface displacement contours produced by the models and the coal horizon contours were transformed to 3-D elevation models, as shown in Figure 6.

The 3-D elevation models are similar but not identical with the observed topography. Both modeled topographies show the elevation changes that clearly outline footwall uplift and hanging wall subsidence, and the small uplift on the hanging wall, east of the fault trace (Fig. 6.a and 6.b.). The hanging wall subsidence produced by the model I (Fig. 6a), is wider and its shape corresponds better with the observed one (Fig. 6c). The beginning of the relay ramp between the two segments is more clearly illustrated by model I. The small depressions observed on the footwall block and in some other locations farther from the vicinity of the fault segments, as well as other topographic differences, are attributed to erosional processes and the integrate history of faulting in the area, factors that were not accounted in the modeling.

Considering all the above, we conclude that the model with the two similar segments (model I) provides the most satisfactory results capturing the overall topography in the fault vicinity.

5.3 STRESS DISTRIBUTION

Since model I is closer to our field data, this model is used for the calculation of the maximum Coulomb shear stress. In the model, fault slip deforms the material around the fault and perturbs the local stress field. The distribution of the perturbed maximum Coulomb shear stress, $\Delta S_{c,}$ in the vicinity of the two overlapping segments illustrates the three dimensional variation in the stress field, especially near the fault tip lines. Normalized to its remote value, ΔS_c is a measure of the stress perturbation around the fault.

Horizontal slices through the model at the depths of 50, 500 and 1000 m are shown in Figure 7(a, b, c). The contours show the distribution of maximum Coulomb shear stress normalized to its remote value. By examining the shallower slice (50 m depth; Fig. 7a), the asymmetric distribution of the Coulomb stress is evident. Regions of relatively high ΔS_c follow the tip lines of the segments and the highest increase is at the segment tips. In the footwall, the maximum Coulomb stress is less than the remote value in contrast with the hanging wall where the Coulomb stress is increased, except in the vicinity of the two segments.

For the intermediate depth (500 m; Fig. 7b) the footwall – hanging wall asymmetry is decreased

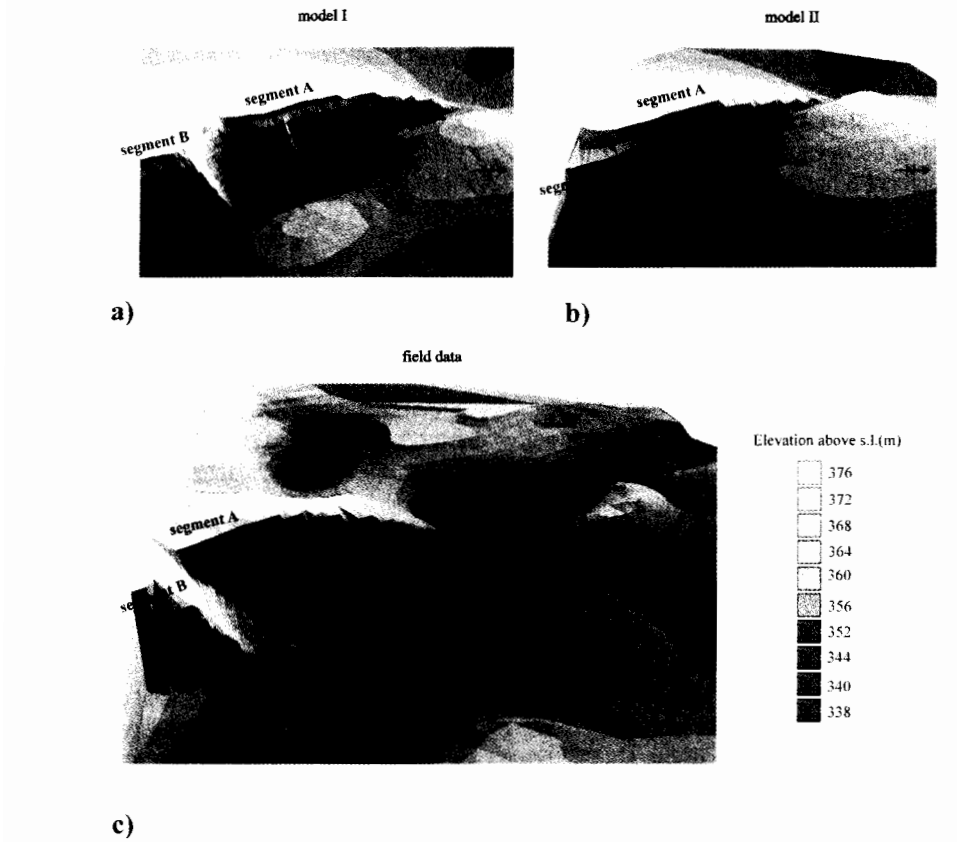

Figure 6. Natural and modeled topography. a) Topography relief produced from the model I b) Topography relief produced from the model II. c) Natural topography of the upper horizon of coal seam III coming from the coal mine data.

and ΔS_c is reduced in that regions relative to the remote value, especially in the footwall. In the relay zone, the effect of segment interaction is clearly visible: ΔS_c in the relay zone is more than the remote value. At the two neighboring tips the stress increase is approximately 160% whereas at the distant tips the stress increase is 140% of the remote value.

At greater depth (1000 m; Fig. 7c), the distribution of stress perturbation is not greatly altered. The magnitude of the stress increase near the tips is 160% and in the relay zone is 120% of the remote value. The only difference is a zone of increased stress into the footwall of the two segments.

To illustrate more clearly the stress perturbation with depth, we constructed a vertical cross section through the center of the relay zone (Fig. 7d). In this section the stress concentration at the tips of both modeled segments is visible. In the relay zone the greatest stress increase is observed in the vicinity of the segment A tip and the stress progressively decreases towards the segment B. Under the depth of ca. 1000 m the contours illustrate a zone of increased stress connecting the two segment tips, creating a "bridge" across the relay. If the stress increase is sufficient, faults and fractures may form in this region, breaching the relay. Thus we see that breaching deformation is more likely to initiate at this depth from the hang-

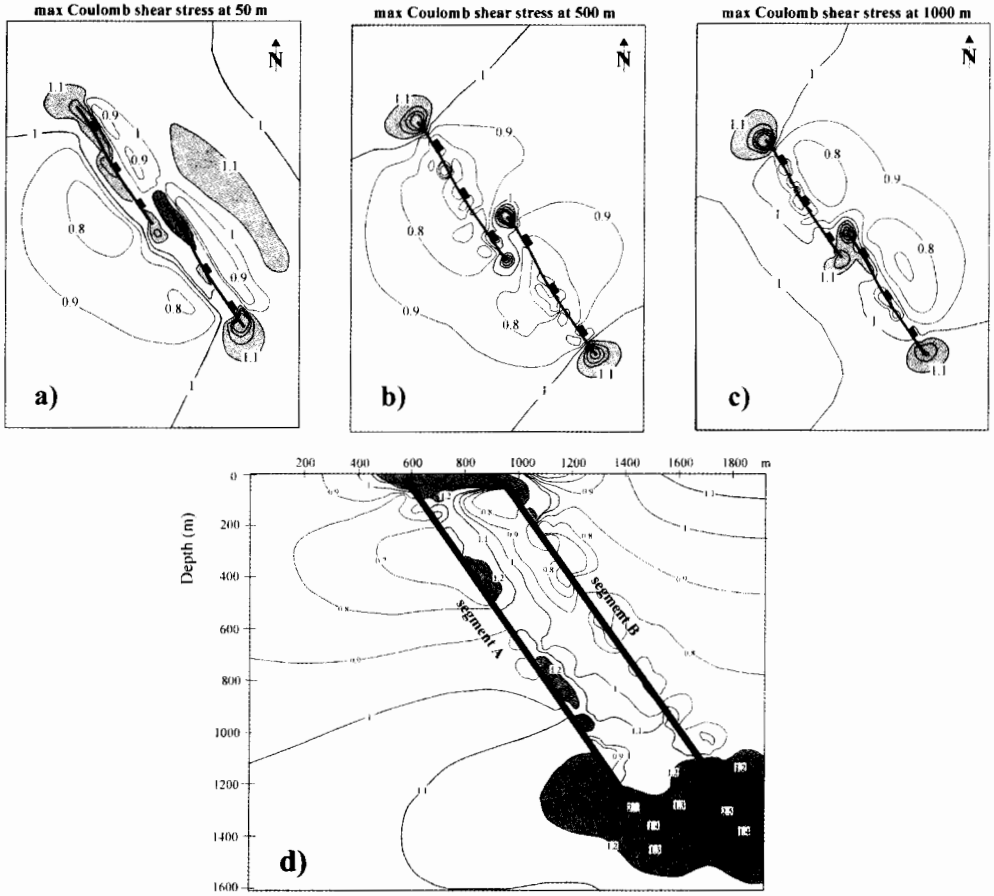

Figure 7. Plan views of the perturbed maximum Coulomb shear stress, ΔS_c, distribution at depths of a) 50m b) 500m and c) 1000m. d) Cross section through the center of the relay zone. Values are normalized to the remote value. Shaded areas indicate where Coulomb stress is increased relative to remote value. Contour interval is 0.1 m.

ing wall of the segment A towards the footwall of the segment B.

6. CONCLUSIONS

Numerical modeling has become a common approach for understanding fault mechanics. We used modeling to show the 3-D distribution of slip on overlapping normal fault segments and how this affects the displacement and stress field of the surrounding rock. Mechanical interaction occurs through local perturbation of the stress field leading to systematic deviations from simple symmetric slip distributions. For the model I which is closer to our observations, the slip distribution on the segments A and B is asymmetric, the area of maximum slip is not located at the center of the segments and the slip gradient in the relay zone is decreased. These results are in agreement with other studies (Willemse 1997, Crider & Pollard 1998) and suggest that segments with appreciable overlap will tend not to propagate.

Slip variation on the segment surfaces and the 3-D shape of the segments influence the stress field in the surrounding material and indicate the way stress is concentrated in the relay zone. The 3-D numerical modeling allows us to use curving

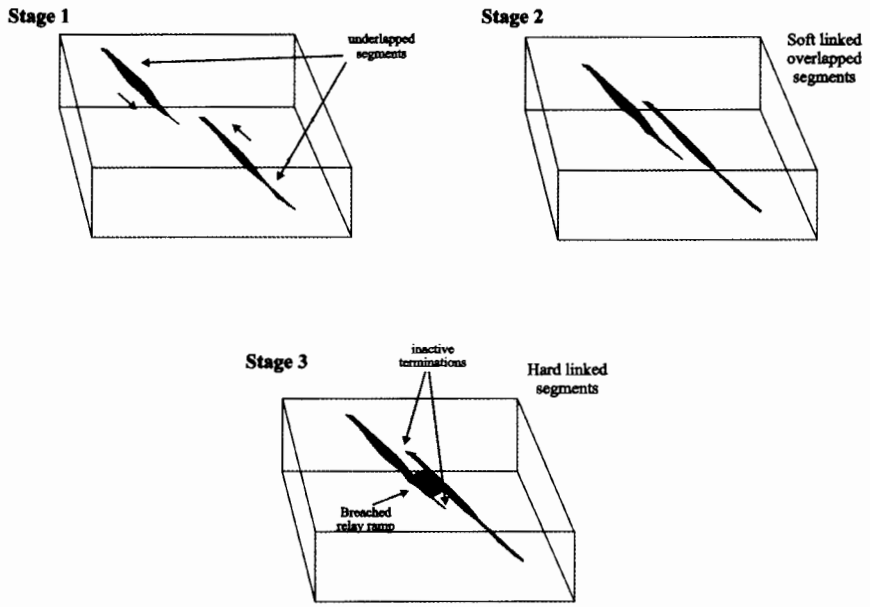

Figure 8. Fault segmentation and linkage. Isolated segments (stage 1) propagate and interact forming relay zones (stage 2). The relay zone is breached to produce a single fault (stage 3).

tip lines; thus the proximity of the fault tips is not everywhere the same. Realistic tip line shapes and not uniform slip distribution on fault surfaces are important differences from other quasi-static stress solutions that have been used to evaluate stress-triggering phenomena of earthquakes (King et al. 1994). In those analyses very small changes in Coulomb stress (˜0.01 Mpa) are correlated with aftershock distributions (Hardebeck et al. 1998). Given the sensibility of these analyses, spatial variation in the stress field due to tip-line shape and slip distribution should be important in predicting stress triggering.

According to several researchers (Cartwright et al. 1995, Kim & Sanderson 2005, Peacock & Sanderson 1991, Wu & Bruhn 1994) three stages can be identified in the growth of fault segments (Fig. 8). Initially isolated segments (stage 1) can propagate towards each other. At stage 2 the fault segments approach each other and interact without obvious connection (soft linkage) producing a relay ramp. Stage 3 is when connecting fractures start to breach the relay ramp producing a single irregular fault (hard linkage) leaving the adjacent segment tips inactive. In this study which provides a mechanical rationale for this sequence of evolution, the segments are soft linked. There is a ramp between them, but the ramp is not breached yet. Slip on the overlapping segments perturbs the local stress field, elevating the maximum Coulomb shear stress in the relay zone and enhancing the likelihood of relay breaching structures. The zone of increased Coulomb stress is observed under the depth of 1000 m, is broader in the footwall and the hanging wall of the segment A and continues to the footwall of the segment B. Under this loading configuration, the greatest potential for deformation is at the depth of 1200 – 1400 m, from the hanging wall of the segment A towards the footwall of the segment B, leading the segments to hard linkage. In this way the breach may be produced solely by the local stress perturbation.

Finally, this study brings together two sets of independent observations, field and numerical. The modeled topography, which represents many identical slip events, is benchmarked against a natural

example. The model reproduces the overall geometry, as well as the footwall and hanging wall deformation. The difference between the modeled and the natural example reflects surface processes and faulting parameters, such as erosion, spatial variations in material properties, development of permanent strains in the host rock material, inelastic deformation near the fault tips, effects of fault growth, friction, etc. All these factors have not included in the model. Further study of the differences between modeled and observed scarp profiles may provide additional insight into the development and degradation of fault scarps. Nonetheless, given the simple nature of the model idealization, the good correspondence between our model and the field data is encouraging.

REFERENCES

Aydin A., Schultz R.A., 1990. Effect of mechanical interaction on the development of strike slip faults with echelon patterns. Journal of Structural Geology, 12, 123-129.

Becker A. A., 1992. The boundary element method in Engineering. McGraw-Hill. New York.

Byerlee J. 1978. Friction of rocks. Pure and Applied Geophysics, 116, 615-126.

Cartwright J.A., Trudgill B.D. and Mansfield C.S., 1995. Fault growth by segment linkage; an explanation for scatter in maximum displacement and trace length data from the Canyonlands Grabens of SE Utah. Journal of Structural Geology, 17, 1319-1326.

Crider J.G. and Pollard D.D., 1998. Fault linkage: 3D mechanical interaction between overlapping normal faults. Journal of Geophysical Research, 103, 24373-24391.

Crider J.G., 2001. Oblique slip and the geometry of normal-fault linkage: mechanics and a case study from the Basin and Range in Oregon. Journal of Structural Geology, 23, 1997-2009.

Crouch S.L. and Starfield A.M., 1990. Boundary Element Methods in solid Mechanics. Unwin Hyman, Boston, Mass.

Comninou M.A., and Dunders J., 1975. The angular dislocation method in a half space. Journal of Elasticity, 5, 203-216.

Dawers N. H., Anders M.H. and Scholz C.H., 1993. Growth of normal faults: Displacement-length scaling. Journal of Structural Geology, 17, 607-614.

Doutsos T. and Kokkalas S., 2001. Stress and deformation patterns in the Aegean region. Journal of Structural Geology, 23, 455-472.

Hardebeck J.L., Nazareth J.J. and Hauksson E., 1998. The static stress change triggering model: Constraints from two southern California aftershock sequences. Journal of Geophysical Research, 103, 24427-24438.

Hiltermann H. and Luttig G., 1969. Biofazies und Paleolimnologie der Pliozanen und Pleistozanen Seen im Megalopolis-Becken (Peloponnes). Mitt. Int. Ver. Limnol., 17, 306-314.

Jaeger J.C. and Cook N.G.W., 1979. Fundamentals of Rock Mechanics. Chapman and Hall, New York.

Jeyakumaran M., Rudnicki J.W., and Keer L.M., 1992. Modeling slip zones with triangular dislocation elements. Bull. Seismol. Soc. Am., 82, 2153-2169.

Kim Y.S. and Saderson D.J., 2005. The relationship between displacement and length of faults: a review. Earth-Science Reviews, 68, 317-334.

King G.C.P., Stein R.S. and Lin J., 1994. Static stress changes and the triggering of earthquakes. Bull. Seismol. Soc. Am., 84, 935-953.

Kokkalas S., Xypolias P., Koukouvelas I. and Doutsos T., 2006. Post Collisional Contractional and Extensional Deformation in the Aegean region. In Dilek. Y, Pavlides S. (eds). Post Collisional Tectonics & Magmatism in the Eastern Mediterranean Region. Geological Society of America Special Paper, (in press).

Koukouvelas I.K., Asimakopoulos M. and Doutsos Th.T., 1999. Fractal characteristics of active normal faults: an example of the eastern Gulf of Corinth, Greece. Tectonophysics, 308, 263-274.

Lohnert E. and Nowak. H., 1965. Die Braunkohlenlagerstaette van Khoremi im Becken von Megalopolis / Peloponnes. Geologishes Jahrbuch, 14, 847-867.

Moore J.M., 1979. Tectonics of the Najd transcurrent fault system, Saudi Arabia. J. Geol. Soc. London, 136, 441-452.

Nelson. R.A., Patton. T.L. and Morley C.K., 1992. Rift segment interaction and its relation to hydrocarbon exploration in rift systems. Buletin of the American Association of Petoleum Geologists, 76, 1153-1169.

Peackock D.C.P., 1991. Displacement and segment linkage in strike-slip fault zones. Journal of Structural Geology, 13, 1025-1035.

Peackock D.C.P. and Sanderson D.J., 1991. Displacements, segment linkage and relay ramps in normal fault zones. Journal of Structural Geology, 13, 721-733.

Peackock D.C.P. and Sanderson D.J., 1994. Geometry and development of relay ramps in normal fault systems. AAPG Bull., 78, 147-165.

Peackock D.C.P., 2002. Propagation, interaction and linkage in normal fault systems. Earth-Science Reviews, 58, 121-142.

Pollard D.D. and Aydin A., 1984. Propagation and linkage of oceanic ridge segments. Journal of Geophysical Research, 89, 10017-10028.

Poulimenos G. and Doutsos T., 1997. Flexural uplift of rift flanks in central Greece. Tectonics, 16, 912-923.

Rippon J.H., 1985. Contoured patterns of throw and hade of normal faults in the coal measures (Westphalian) of northeast Derbyshire, Proc. York. Geol. Soc., 45, 147-161.

Segall P. and Pollard D.D., 1980. Mechanics of discontinuous faults, Journal of Geophysical Research, 85, 4337-4350.

Tchalenko J.S. and Ambraseys N. N., 1970. Structural analysis of Dasht-e Bayaz (Iran) earthquake fractures. Geol. Soc. Am. Bull. , 81, 41-60.

Thomas A.L., 1993. Poly3D: a three dimensional , polygonal-element, displacement discontinuity boundary element computer program with applications to fractures, faults, and cavities in the Earth's crust. M.S. thesis, Standford University, California.

Van Vugt N., 2000. Orbital forcing in late Neogene lacustrine basins from the Mediterranean. A magnetostratigraphic and cyclostratigraphic study. Ph.D thesis, Utrecht University. Geologica Ultraiectina, 189, 167.

Vinken R., 1965. Stratigraphic und Tektonik des Beckens von Megalopolis (Peloponnes, Griecheland). Geologishes Jahrbuch, 83, 97-148.

Willemse E.J.M., Pollard D.D., and Aydin A., 1996. 3D analyses of slip distribution on normal faults arrays with consequences for fault scaling. Journal of Structural Geology, 18, 295-309.

Willemse E.J.M., 1997. Segmented nomal faults: correspondence between three-dimensional mechanical models and field data. Journal of Geophysical Research, 102, 675-692.

Wu D. and Bruhn R.L., 1994. Geometry of and kinematics of active normal faults, South Oquirrh Mountains, Utah: Implications for fault growth. Journal of Structural Geology, 16, 1961-1975.

3-D ΑΡΙΘΜΗΤΙΚΗ ΠΡΟΣΟΜΟΙΩΣΗ ΕΠΙΚΑΛΥΠΤΟΜΕΝΩΝ ΤΜΗΜΑΤΩΝ ΚΑΝΟΝΙΚΩΝ ΡΗΓΜΑΤΩΝ: ΕΝΑ ΠΑΡΑΔΕΙΓΜΑ ΑΠΟ ΤΗ ΛΕΚΑΝΗ ΜΕΓΑΛΟΠΟΛΗΣ, ΠΕΛΟΠΟΝΝΗΣΟΣ, ΕΛΛΑΔΑ

Σούρλας Γ., Κοκκάλας Σ., Κουκουβέλας Ι.
Τμήμα Γεωλογίας, Πανεπιστήμιο Πατρών, 26500, Πάτρα, Ελλάδα.

Περίληψη

Πολλά από τα κανονικά ρήγματα αποτελούνται από επικαλυπτόμενα τμήματα. Τα δεδομένα υπαίθρου ενεργών και ανενεργών ρηγμάτων δείχνουν ότι η κατάτμηση των ρηγμάτων επιδρά στην κατανομή της ολίσθησης επί του ρήγματος. Η κατανομή της ολίσθησης είναι πολύπλοκη και ασύμμετρη και συνήθως η θέση μέγιστης ολίσθησης δεν συμπίπτει με το γεωμετρικό κέντρο των τμημάτων του ρήγματος. Στις ζώνες μεταβίβασης η βαθμίδα της μετατόπισης είναι μεγαλύτερη όπως συνάγεται για

ένα παράδειγμα στα λιγνιτικά πεδία της Μεγαλόπολης όπου εφαρμόστηκε η αριθμητική προσομοίωση σε δύο επικαλυπτόμενα τμήματα ρήγματος. Η αριθμητική προσομοίωση έδειξε τη δημιουργία ασύμμετρων κατανομών ολίσθησης στα δύο γειτονικά τμήματα του ρήγματος και αλλαγές στο πεδίο των τάσεων χωρίς τα δύο τμήματα του ρήγματος να αποτελούν το ένα συνέχεια του άλλου. Επιπλέον η αριθμητική προσομοίωση επιτρέπει την αναπαράσταση των κύριων χαρακτηριστικών των ρηξιγενών πρανών και την κατανομή της τάσης Coulomb γύρω από το ρήγμα. Οι περιοχές όπου αυξάνεται η τάση Coulomb παρουσιάζουν την πιθανότητα φυσικής συνένωσης των τμημάτων των ρηγμάτων.